PCCP

Accepted Manuscript

ROYAL SOCIETY OF CHEMISTRY

www.rsc.org/pccp

Internal Conversion and Intersystem Crossing in α,β-Enones: A Combination of Electronic Structure Calculations and Dynamics Simulations

Jun Cao[abc], Zhi-Zhong Xie*[d]

[a]*Guizhou Provincial Key Laboratory of Computational Nano-material Science, Guizhou Education University, Guiyang, Guizhou, 550018, China*

[b]*Guizhou Synergetic Innovation Center of Scientific Big Data for Advanced Manufacturing Technology, Guizhou Education University, Guiyang, 550018, China*

[c]*Key Laboratory of Theoretical and Computational Photochemistry, Ministry of Education, College of Chemistry, Beijing Normal University, Beijing 100875, China*

[d]*Department of Chemistry, School of Chemistry, Chemical Engineering and Life Sciences, Wuhan University of Technology, Wuhan 430070, China*

The ab initio electronic structure calculations and CASSCF-based nonadiabatic dynamics simulations have been used to investigate the internal conversion and intersystem crossing process of both *trans*-acrolein and 2-cyclopentenone in the gas phase. Our calculation results show that relaxation from the Franck-Condon region to a S_1 minimum is ultrafast, and that the S_1 state will dominantly undergo intersystem crossing to triplet states due to the existence of significant barriers to access the S_1/S_0 intersection points and of energetically close-lying triplet states. The $S_1/T_2/T_1$ three-state intersection is observed in our dynamics simulations to play an important role in population of the lowest triplet state, which is consistent with previous suggestions. Although the evolution into triplet states involves the similar path and gives rise to a similar triplet quantum yield for these two molecules, the intersystem crossing rate of 2-cyclopentenone is lower owing to the ring constraint that results in a smaller spin-orbital coupling in the singlet-triplet crossing region. The present theoretical study reproduces the experimental results and gives an explanation about the structural factors that rule the excited-state decay of some types of α,β-enones.

Introduction

α,β-Enones are a class of molecules containing two direct linked functional

groups: ethylenic (CH2=CH–) and carbonyl (–HC=O) group. Among the α,β-enone derivatives, acrolein (AC) is the smallest acyclic α,β-enones, which has been observed in interstellar space[1] and found in cigarette smoke and automobile exhaust.[2] Moreover, AC was known to exert different biologic effects through reactions with cellular macromolecules to give adducts, some of which are potentially involved in human cancers.[3,4] 2-Cyclopentenone (CPO) is a cyclic α,β-enone molecule, and the organic photochemistry of cyclic enones has received considerable interest due to their applications in organic synthesis.[5,6]

Upon UV excitation, α,β-enones showed a variety of photoinduced processes. Several works were devoted to the photodissociation of AC under irradiation with wavelengths in the range of 288–334 nm,[7–9] and three product channels, that is, CH3CH + CO, CH2CH + CHO, and CH2CHCO + H, were identified as major. The ultraviolet photodissociation of AC upon excitation into the S_2 state with wavelength 193 nm has also been studied experimentally in some details[10–18] and six dissociation channels were observed. Fifteen photofragments upon photolysis of AC at 193 nm were even observed using photofragment translation spectroscopy and selective vacuum-ultraviolet photoionization.[19] Theoretically, Fang computed the S_0, S_1 and T_1 potential energy surfaces (PESs) of AC for the gaseous photodissociation.[20] Reguero *et al.*[21] performed computational investigations of the photophysics of *trans*-acrolein following photoexcitation, and showed that the S_1 state decays via a series of crossing points to the $T_1(\pi\pi^*)$ state. In the solution-phase environment, [1,3] H-migration was observed to be the major channel with a product yield of 0.78 and was suggested to take place on the $T_1(\pi\pi^*)$ state of AC.[22] For CPO and related cyclic α,β-enones, their typical photo-induced reactions include cycloaddition, hydrogen abstraction, and rearrangements, and have been investigated in many experiments[23–29] and theoretical calculations.[30–33] These works provided important insights into the multi-channel photodissociation and photoisomerization mechanisms of α,β-enones, and emphasized the significant role played by the internal conversion (IC) and intersystem crossing (ISC) in these reactions. Small yields of fluorescence and phosphorescence of

α,β-enones have also been reported and explained in terms of the rapid IC to ground state and/or ISC to triplet states that lies close to the first excited singlet state.[34]

The intramolecular electronic relaxation processes in some α,β-enones have been investigated using time-resolved and cavity ringdown spectroscopy.[17,35–38] These experiments indicated that ISC is able to efficiently compete with IC in most of the simple enones upon optical excitation to the S_2 state. Furthermore, ISC is the only observed relaxation pathway upon direct excitation to the S_1 state.[20,29] Recently, Schalk et al.[39] investigated the nonradiative relaxation pathways of CPO and its methylated derivatives, as well as the open chain molecule MVK, by means of time-resolved photoelectron spectroscopy, and found that the molecule subsequently decays to the triplet manifold and the singlet ground state, with quantum yields of 0.35 and 0.65, respectively, upon excitation to the S_2 state.

Previous static electronic structure calculations, including optimizations of minima, transition states, and conical intersections (CIs), are very helpful for understanding the mechanism of photochemical reactions of enone.[20,21] In fact, the photophysics and photochemistry of α,β-enones involve a complicated process in which many electronic states interact and overlap with one another. Thus it would be beneficial to investigate these interactions with a combination of electronic structure calculations and dynamics simulations, providing additional insights to the complicated excited-state decay dynamics. In this study, we took AC and CPO as representative model systems, and attempted to elucidate the atomic details, time scales, and factors that affect the rate and efficiency of both IC and ISC upon excitation to the S_1 state by a combination of advanced electronic structure calculations and ab initio based dynamics simulations.

The present calculations show that relaxation from the Franck–Condon (FC) region to a S_1 minimum is ultrafast, and that the $S_1/T_2/T_1$ three-state intersection plays an important role in population of the T_1 state. Although the evolution into triplet states involves the similar path and gives rise to a similar triplet quantum yield (0.8) for these two molecules, the intersystem crossing rate of CPO is lower owing to the

ring constraint that results in a smaller spin–orbital coupling (SOC) in the singlet-triplet crossing region. The present theoretical study reproduces the experimental results and gives an explanation about the structural factors that rule the excited-state decay of some types of α,β-enones.

Computational Details

Electronic Structure Calculations. All stationary geometries on the S_0, S_1, T_1 and T_2 state PESs were fully optimized with the complete active space self-consistent field (CASSCF) energy gradient method. Points of surface crossing among different electronic states were determined by the state-averaged (SA) CASSCF calculations.[40,41] For the optimized equilibrium and transition state geometries, the nature of stationary points was confirmed by an analytical frequency computation. The optimization calculations described above were carried out with the Gaussian 09 software package,[42] and the Molpro 2010.1 software package[43] was applied in optimization of the singlet/triplet crossing points and dynamics simulation. The SOC constants were computed at the optimized singlet/triplet crossing points using the atomic mean-field approximation (AMFI)[44,45] as implemented in the Molpro 2010.1 software package.

To describe equilibrium structures of both AC and CPO in low-lying electronic states, one needs the π and π* orbitals of both C=C and C=O groups and a nonbonding molecular orbital on the oxygen atom, that is, 6 electrons in 5 orbitals, referred to as CAS(6,5) hereafter. For CPO, additional σ and σ* orbitals between the carbonyl carbon and an sp3-ring carbon atom were included in the active space, referred to as CAS(8,7) hereafter.

It is well known that the relative energies are usually overestimated by the CASSCF calculation, and it is necessary to take a correction to energies by the inclusion of dynamic correlation. The multiconfigurational second-order perturbation theory (CASPT2) approach[46–48] is a very efficient algorithm for treating dynamic correlation. To refine the relative energies of the CASSCF optimized structures, single-point energies were calculated using the CASPT2 method as implemented in

MOLCAS 8.0 software package.[49] To achieve a balanced description of the states in the CASPT2 calculation, the multi-state (MS) CASPT2 method[50] was applied when more than one state was considered. Also, the imaginary shift technique (0.2 a.u.) was employed to avoid intruder state issues in CASPT2 calculations.[51] All calculations were performed with 6-31G* basis set. Furthermore, based on the CASSCF/6-31G* optimized structures, CASPT2 single-point calculations with ANO basis set have also been conducted. As shown in Tables S1 and S2 of Supporting Information, the relative energies are not sensitive to the basis sets too much.

Details of dynamics simulation. The nonadiabatics dynamics simulations were carried out with an in-house ab initio molecular dynamics code,[52,53] which was designed to interface to the Gaussian 09 and Molpro 2010.1 software packages. In the dynamics simulations, the nuclear trajectories evolve always on a single adiabatic surface, and the nonadiabatic events were taken into account by means of Tully's fewest-switches surface hopping (FSSH) algorithm.[54] When the spin-orbital (SO) interactions between the singlet and triplet states should also be taken into account, the non-relativistic electronic Hamiltonian can be defined as

$$\hat{H}^{el}(\mathbf{r},\mathbf{s},\mathbf{R}(t)) = \hat{H}^{SF}(\mathbf{r},\mathbf{R}(t)) + \hat{H}^{so}(\mathbf{r},\mathbf{s},\mathbf{R}(t)), \quad (1)$$

where $\hat{H}^{SF}$ is the spin-free part of Hamiltonian, $\hat{H}^{so}$ is the spin-orbital interaction term, and **r** and **s** correspond to spatial and spin coordinates of electrons. The time-dependent Schrödinger equation now can be written down as

$$i\hbar\frac{\partial\Psi(\mathbf{r},\mathbf{s},\mathbf{R}(t),t)}{\partial t} = \left(\hat{H}^{SF}\left(\mathbf{r},\mathbf{R}(t)\right) + \hat{H}^{so}\left(\mathbf{r},\mathbf{s},\mathbf{R}(t)\right)\right)\Psi(\mathbf{r},\mathbf{s},\mathbf{R}(t),t). \quad (2)$$

The time-dependent electronic wave function can be expressed in terms of the eigenvectors of $\hat{H}^{SF}$,

$$\Psi(\mathbf{r},\mathbf{s},\mathbf{R}(t),t) = \sum_k c_k(t)\varphi_k\left(\mathbf{r},\mathbf{s},\mathbf{R}(t)\right). \quad (3)$$

After inserting Eq. (3) into Eq. (2), multiplying by $\varphi_k^*(\mathbf{r},\mathbf{s},\mathbf{R}(t))$ from the left-hand side, and integrating over electronic coordinates, we obtain the system of coupled equation for the time evolution of the expansion coefficients of the electronic basis function

$$i\hbar\frac{\partial c_k(t)}{\partial t} = c_k(t)V_k(\mathbf{R}(t)) + \sum_j c_j(t)\left(\mathrm{H}_{kj}^{SO}(\mathbf{R}(t)) - i\hbar\dot{\mathbf{R}}(t)\cdot\mathbf{d}_{kj}(\mathbf{R}(t))\right) \quad (4)$$

where $\mathrm{H}_{kj}^{SO}(\mathbf{R}(t)) = \left\langle \varphi_k(\mathbf{r},\mathbf{s},\mathbf{R}(t))\middle|\hat{H}^{so}\middle|\varphi_j(\mathbf{r},\mathbf{s},\mathbf{R}(t))\right\rangle$ is the SOC matrix element between electronic states k and j at nuclear coordinates $\mathbf{R}(t)$, $\mathbf{d}_{kj}(\mathbf{R}(t)) = \left\langle \varphi_k(\mathbf{r},\mathbf{s},\mathbf{R}(t))\middle|\nabla_R\varphi_j(\mathbf{r},\mathbf{s},\mathbf{R}(t))\right\rangle$ is the nonadiabatic coupling vectors, and $V_k(\mathbf{R}(t)) = \langle\varphi_k(\mathbf{r},\mathbf{s},\mathbf{R}(t))|\hat{H}^{SF}|\varphi_k(\mathbf{r},\mathbf{s},\mathbf{R}(t))\rangle$. It should be noted that, $\mathbf{d}_{kj}(\mathbf{R}(t))$ is zero when state k is the same as state j or both states are of different spin multiplicity.

Then, the hopping probability from state k to state j can be written down as

$$P_{k\to j}(t) = 2\int_t^{t+\Delta t} d\tau \frac{Im\left[c_j(\tau)c_k^*(\tau)\mathrm{H}_{kj}^{SO}(\tau)/\frac{h}{2\pi}\right] - Re\left[c_j(\tau)c_k^*(\tau)\dot{\mathbf{R}}\cdot\mathbf{d}_{jk}(\tau)\right]}{c_k(\tau)c_k^*(\tau)}. \quad (5)$$

It is noted that, the original Tully's FSSH has only been formulated to deal with the IC process, but Eq. (5) can be used to take into account both IC and ISC processes simultaneously in a dynamic simulation calculation. That is, in Eq. (5) an additional term, $Im\left[c_j(\tau)c_k^*(\tau)\mathrm{H}_{kj}^{SO}(\tau)/\frac{h}{2\pi}\right]$, was introduced to mediate the hopping between electronic states of different spin multiplicity.

In fact, the SO interaction has previously been taken into account in many trajectory calculations, including classical and quantum wavepacket simulations, of multi-state reaction and photodissociation dynamics, but most of which are based on the use of pre-computed PESs and some types of SOC approximations.[55–65] Combined with Tully's FSSH, Granucci *et al.*[66–68] provided two algorithms in both spin-diabatic and spin-adiabatic representations and investigated their merits and limitations for model systems. Cui *et al.*[69] also present a generalized trajectory surface-hopping method for simulating both IC and ISC processes. Richter *et al.*[70–72] formulated a general FSSH method which resort to a unitary transformation between diabatic and adiabatic representations to enable the treatment of SOC and other types of couplings.

Eq. (5) is the central formula used in our trajectory calculations. As stressed by Granucci *et al.*,[66] in the spin-diabatic approach the total intermultiplet transition probability between two states of different spin should be rotationally invariant, and it

can be achieved by assuming that each spin multiplet can be considered as a single electronic state. As a matter of fact, this approximation has commonly been used in previous studies of SOC-mediated processes.[55,57,60,62,64,65] This is a good approximation for organic molecule, and it simplifies our ISC dynamics treatment. In present implement, we adopt this approximation and determine an effective SOC value as the root mean squared coupling constant as the strength of SO interaction between the two interacting multiplets.

The nuclear trajectories were investigated using the velocity-Verlet algorithm with the time step of 0.5 fs. At each new generated structure, the energies, gradients, and nonadiabatic coupling vectors $\mathbf{d}_{kj}$, as well as SOC constants, were computed at the state-averaged CASSCF level. For propagation of the electronic wave function, the fourth-order Runge-Kutta method was used with the integration step of 0.01 fs, where the energies, velocities, and nonadiabatic coupling vectors, as well as SOC constants, were linearly interpolated for the intermediate steps. Finally, the nonadiabatic transition probability between different electronic states can be computed. In the case of hopping, the nuclear velocities were adjusted in the direction of the gradient difference vectors to conserve the total energy of the system.

The initial geometries and velocities for the photodynamics simulations of these two molecules in the gas phase were generated by a Wigner distribution for the quantum harmonic oscillator in the specified ground vibrational state at the ground electronic states. The maximum simulation time of each trajectory was initially set to 10 ps for AC, and 20 ps for CPO. Due to the omitting of the possible isomerization events on the S_0 or T_1 state, we determined to terminate a trajectory calculation if the trajectory passes the intersection/crossing point and resides in the S_0 or T_1 state for about 100 fs. The trajectory calculations of both AC and CPO were performed at the SA2-CAS(6,5)/6-31G* and SA2-CAS(8,7)/6-31G* level, respectively.

Results and Discussions

Equilibrium structures and their relative energies. The optimized equilibrium geometries of AC and CPO in the S_0, S_1, T_1 and T_2 state, and their relative energies

were shown in Figures 1 and 2, respectively. The Cartesian coordinates and relative energies of these optimized structures were given in parts of S1, S2, and Tables S1 and S2 of Supporting Information.

As can be seen in Figure 1, for the minimum of AC in the S_0 state, referred to as AC_S_0 hereafter, the optimized bond-lengths of the C=O, C−C, and C=C bond agree well with the experimental values.[73] For CPO, the CAS(8,7) calculated ground-state structure, referred to as CPO_S_0 in Figure 2, gives rise to rotational constants of $\bar{A}$ = 7.431 GHz, $\bar{B}$ =3.582 GHz, and $\bar{C}$ =2.490 GHz, which may be compared to the experimental microwave values of 7.410, 3.586, and 2.493 GHz.[74] Both AC and CPO in the ground state have a central C−C bond of higher bond order than a single bond, due to conjugative effects between the C=C and C=O group. Similar to the optimized S_0 minima, the excited state minima also have a C_s symmetry with the molecular plane as the mirror plane, but the C2−C3 bond shrinks further compared to the ground state. The shrinking of the C2−C3 bond on excited states results in a higher barrier for the trans-cis isomerization around the C2−C3 bond, which implies that the trans-cis isomerization was not easy to occur on the excited states.[21,34] The ab initio calculations also showed that the lowest $^3\pi\pi^*$ state minimum of AC has a diradical electronic structure, and that the terminal CH2 group twists 90° out of the molecular plane, resulting in the $T_1(\pi\pi^*)$ state is ca. 10 kcal/mol lower than the $T_1(n\pi^*)$ state minimum. Whereas, this type of conformational change is not so large in CPO due to the geometrical constraints of the ring, thus the two triplet states are seen to be nearly isoenergetic, which is consistent with the spectroscopic observations.[25,28]

The computed $S_0 \rightarrow S_1(n\pi^*)$ vertical excitation energy of AC is 91.3 kcal/mol by the CASPT2//CAS(6,5)/6-31G* calculation, which reproduces the measured value of 331.5 nm (86.3 kcal/mol).[34] For CPO, the $S_0 \rightarrow S_1(n\pi^*)$ vertical excitation energy was computed to be 89.5 kcal/mol at the CASPT2//CAS(8,7)/6-31G* level, which is in reasonable agreement with the experimental observation.[38,39] The S_1 minimum of AC, referred to as AC_S_1 hereafter, was predicted to have a relative energy of 76.0 kcal/mol by the CASPT2//CAS(6,5)/6-31G* calculation compared to AC_S_0, and for

CPO the relative energy of the S_1 minimum (CPO_S_1) is 78.5 kcal/mol at the CASPT2//CAS(8,7)/6-31G* level.

The S_1 State Decay of AC. The optimized geometries of the minimum energy conical intersection (MECI) points connecting S_1 with S_0, and T_2 with T_1, and the minimum energy crossing points (MECP) connecting S_1 with T_2, and S_0 with T_1, were displayed in Figure 1(a), and the corresponding schematic potential energy profile was plotted in Figure 1(b). Also, the Cartesian coordinates and energies of these optimized structures were given in parts of S1 and Table S1 of Supporting Information.

After initial relaxation from the FC region to a S_1 minimum, the molecule may decay through either IC to the electronic ground state or ISC to the triplet manifold.[20,21] The S_1 state has a conical intersection with the S_0 state at a geometry with 90°-twisted ethylenic C=C coordinate, referred to as AC_S_1S_0 hereafter. This MECI was located about 20.0 kcal/mol above AC_S_1. A similar barrier of 17.3 kcal/mol was reported for this path.[21] For the triplet decay path of the S_1 state of AC, a MECP point structure between S_1 and T_2, AC_S_1T_2, was optimized. The gradient difference vectors of this crossing point shows that the $S_1 \rightarrow T_2$ transition mainly involves shrinking of the O1−C2 and C2−C3 bond, and stretching out of the C3-C4 bond with respective to the S_1 minimum. By going over AC_S_1T_2, the system can access a MECI between T_2 and T_1, AC_T_2T_1, which is also planar and provides a fast radiationless decay channel from T_2 to T_1. It has been noted that the motion from S_1/T_2 to T_2/T_1 occurs via an in-plane deformation, which essentially involves a bond order inversion with respect to the ground-state structure.[21]

The S_1/T_2 crossing is rather close to the S_1 minimum (~1.0 kcal/mol), thus the facile intersystem crossing at the S_1/T_2 crossing is usually assumed to be ultrafast and occurs very efficiently.[75] However, the efficiency of the ISC process is determined by not only the small energy gap separating the singlet and triplet states, but also the size of SOC and dynamic factors. Therefore, 100 trajectories for dynamic simulation of

the excited state decay of AC have been performed from the FC region of the S_1 state, and 18 trajectories failed due to CASSCF convergence problem.

After close examination to time evolution of the bond parameters (see Figure S1) and potential energies of the electronic states, it was found that all trajectories relax from the S_1 FC region to a structural region of S_1 minimum within ~1000 fs, and then keep oscillation for some periods before crossing the S_1/T_2 or S_1/S_0 point. During this period, both trans-cis isomerization around the central C2−C3 bond (see O1−C2−C3−C4 dihedral angle of Figure S1) and rotation of the terminal CH2 group around the C3−C4 bond were observed (see C2−C3−C4−H8 dihedral angle of Figure S1). After that time, 62 trajectories were observed to undergo a $S_1 \rightarrow T_2$ hop, and 3 trajectories for a $S_1 \rightarrow T_1$ hop. The remaining 17 trajectories decay by a $S_1 \rightarrow S_0$ hop. Below, we will describe these three typical trajectories in some details.

We first address an example of a $S_1 \rightarrow S_0$ hop. Figure 3 shows the time evolution of the potential energies, SOC constants, nonadiabatic couplings, and several key geometric parameters in a representative trajectory. It is seen that the $S_1 \rightarrow S_0$ hopping takes place at 1758.5 fs at which there is a nonadiabatic coupling value of -38.1 ps^{-1} and an energy gap of 12.8 kcal/mol. After returning to the S_0 state, the bond-lengths of the O1−C2 and C2−C3 bond quickly relax to typical ground-state values around 1.21 and 1.34 Å, respectively. In the S_0 state, the hot *trans*-acrolein can also transform into the *cis*- isomer (see O1−C2−C3−C4 dihedral angle). Closer examination of time evolution of the C2−C3−C4−H8 and H7−C3−C4−H8 dihedral angles (see Figure S1) and potential energies for all trajectory of this type shows that a hop from S_1 to S_0 is triggered by a twist-pyramidalization motion, which is consistent with the proposition of Lee et al.[36] They theoretically investigated the S_1 relaxation of some methyl substituented AC in terms of the energetic and topographical features of the S_1/S_0 intersection points, and proposed that the vibrational dynamics occurring near the S_1/S_0 CI is closely associated with the surface crossing probabilities and that torsion about the terminal CHX group is a important factor for sufficient nonadiabatic transition from S_1 to S_0, although the torsion is not one of the two coordinates that

lifts the degeneracy in first order at the MECI.

The second example shows a $S_1 \rightarrow T_2$ hop. As seen from our trajectory calculations, most trajectories (62 trajectories) undergo ISC to reach the triplet state potential energy surfaces. In the trajectory depicted in Figure 4, a $S_1 \rightarrow T_2$ hop takes place at 1930.0 fs when the SOC constant is computed to be 43.6 cm^{-1}. After another 5.5 fs, there is a $T_2 \rightarrow T_1$ hop triggered by a large nonadiabatic coupling of 239.5 ps^{-1}. During this small time interval, the three involved states are almost degenerate in energy, which facilitates the observed sequential nonadiabatic transitions. After another ~80.0 fs (i.e., at 2010.0 fs), AC in the T_1 state starts to twist around the H6−C3−C4−H8 dihedral angle, accompanied by a shortening of the O1−C2 bond and an elongation of the C2−C3 and C3−C4 bonds. These structural changes reflect the evolution into the T_1 state minimum of AC.

The third typical example (see Figure 5) concerns a direct $S_1 \rightarrow T_1$ hop. This type of trajectory is only found rarely (in 3 trajectories). The $S_1 \rightarrow T_1$ hop takes place at 1822.0 fs when there is a large S_1-T_1 SOC of 44.6 cm^{-1} and a small S_1-T_1 energy gap of 1.1 kcal/mol. In the trajectory AC does not access the T_2 state, implying that the T_2 state has no relevance to the dynamics.

The S_1 State Decay of CPO. A MECP between S_1 and T_2 of CPO, CPO_S_1T_2, was optimized, in which the O1−C2 bond-length decreased by 0.03 Å and the C3−C4 bond-length is increased by ~0.07 Å compared to CPO_S_1. Also, a pyramidalization of C6 atom occurs. A planar MECI between T_2 and T_1 of CPO, CPO_T_2T_1, was optimized. Examination to structural parameters of the optimized S_1/T_2 and T_2/T_1 geometries showed that CPO_S_1T_2 is very similar to CPO_T_2T_1 in structure, and both have nearly the same energy.

Along the α-cleavage of the C2−C6 bond, a transition state, referred to as TS_S_1 hereafter, was optimized and confirmed by a frequency calculation. Taking TS_S_1 as an initial guess, a conical intersection between S_1 and S_0, CPO_S_1S_0, was optimized by the SA2-CAS(8,7)/6-31G* calculation. The C2−C6 bond-length increases from 1.964 Å in TS_S_1 to 2.665 Å in CPO_S_1S_0. The CASPT2//CAS(8,7)/6-31G*

calculations predicted that, the barrier to access TS_S_1 is 12.7 kcal/mol, while only ~2.0 kcal/mol for the S_1/T_2 crossing.

A S_1/S_0 conical intersection was optimized and found to be associated with the C2−C3 bond cleavage. The barrier to access this CI is about 40.0 kcal/mol compared to CPO_S_1. All attempts to optimize a S_1/S_0 CI which is similar to the twisted one of AC at the CAS(8,7)/6-31G* level failed, but it was believed that when the rigidity of the system is increased, more energy is required to reach the twisted S_1/S_0 intersection. A barrier of 28.4 kcal/mol (1.23 eV) for the twist-pyramidalization S_1/S_0 MECI of CPO was estimated in previous study.[39]

The optimized MECI and MECP geometries for CPO and corresponding schematic potential energy profile were shown in Figure 2, and the Cartesian coordinates and energies of these optimized structures were given in parts of S2 and Table S2 of Supporting Information.

One hundred trajectories were initially calculated starting from the FC region of the S_1 state of CPO in the gas phase, and 13 trajectories failed due to CASSCF convergence problem. Figure S2 shows the time evolution of some key geometrical parameters for these remaining 87 trajectories. Upon analyzing time evolution of the bond parameters and energies of the excited states, it was found that the initial relaxation of CPO is very similar to AC. That is, upon photo-excitation of CPO into the S_1 state, the molecules make their way toward the S_1 minimum, and this relaxation process is ultrafast and mainly involves stretching of the O1−C2 and C3−C4 bond and shrinking of the C2−C3 bond. After initial relaxation, all trajectories keep oscillation in a structural region of S_1 minimum for a long time before crossing the S_1/T_2 or S_1/S_0 point. Summarily, for CPO, three relaxation pathways that lie below the excitation energy were observed: the familiar twist-pyramidalization at the C3−C4 double bond in the CPO ring (5 trajectories), α-cleavage of the C2−C6 bond (11 trajectories), and ISC to T_2 (66 trajectories) or T_1 (5 trajectories) from S_1. Below, we will describe these four typical trajectories.

We first address a typical example of a $S_1 \rightarrow S_0$ hop. For decay through the twisted S_1/S_0 intersection, this type of trajectory is rare (5 trajectories). Figure 6 shows the time evolution of the potential energies, SOC constants, nonadiabatic couplings, and several key geometric parameters in a representative trajectory. It is seen that a $S_1 \rightarrow S_0$ hop takes place at 1930.0 fs at which there is a nonadiabatic coupling value of -15.1 ps^{-1} and a energy gap of 36.6 kcal/mol. After returning to the S_0 state, the bond-lengths of the O1−C2 and C3−C4 bond quickly relax to typical ground-state values around 1.22 and 1.34 Å, respectively, while the C2−C3 bond-length returns to 1.48 Å. Closer examination of time evolution of the C2−C3−C4−H8 dihedral angle for the representative trajectory shows that, this dihedral angle reaches ~108° at 1400 fs and then oscillates around 150° until a $S_1 \rightarrow S_0$ hop occurs at a geometry in which the C2−C3−C4−H8 dihedral angle is 157.1°. Once hopping to the ground state, large oscillation of the O1−C2−C3−C4 and H7−C3−C4−H8 dihedral angles was also observed. Close examination of the energy gap between S_1 and S_0 at a hop for all of this type of trajectory shows that, the S_1-S_0 energy gap varies from 23 to 42 kcal/mol, and mainly involves out-of-plane of the C2−C3−C4−H8 dihedral angle.

Secondly, we address the other typical example of a $S_1 \rightarrow S_0$ hop. In CPO, the large amplitude rotation distortion of the terminal CH2 group is hindered, thus IC to ground state through the twisted S_1/S_0 intersection is unfavorable. Alternatively, returning to ground state through α-cleavage of the C2−C6 bond is preferable due to a lower barrier (12.7 kcal/mol) to access this path. As seen from Figure 7, a $S_1 \rightarrow S_0$ hop takes place at 4733.5 fs at which there is a large nonadiabatic coupling value of -517.1 ps^{-1} and a small energy gap of 1.1 kcal/mol. After returning to the S_0 state, the C2−C6 bond-length quickly increases, while the C4−C6 bond-length quickly decreases, and they then keep oscillation around 3.8 and 1.45 Å, respectively. Closer examination of time evolution of the geometrical parameters shows that the trajectory traps in the ground state minimum of cyclopropylketenes, referred to as CK_S_0 in Figure 2. In fact, this type of trajectory can also result in returning to the reactant in the ground state when passing the S_1/S_0 CI.

The third example shows the $S_1 \rightarrow T_2$ hop. In the trajectory depicted in Figure 8, a $S_1 \rightarrow T_2$ hop takes place after 5584.5 fs, when the SOC constant is computed to be 25.6 cm^{-1}. After another 11 fs, there is a $T_2 \rightarrow T_1$ IC triggered by a nonadiabatic coupling of -144.4 ps^{-1}. During this small time interval, the three involved states are almost degenerate in energy, which facilitates the observed sequential nonadiabatic transitions. After another about 700 fs (i.e. at 6295 fs), CPO in the T_1 state starts to twist around the C2−C3−C4−H8 and H7−C3−C4−H8 dihedral angles, accompanied by a shortening of the O1−C2 bond and an elongation of the C2−C3 and C3−C4 bonds. In fact, closer examination of time evolution of the geometrical parameters shows that hopping to T_2 involves stretching of the C3−C4 bond and shrinking of the O1−C2 bond, which is consistent with the results of electronic structure calculations.

Figure S3 shows distribution of the energy difference and time interval for those trajectories which undergo a $S_1 \rightarrow T_2$ hop. As seen from Figure S3, these two molecules have similar distribution. That is, the energy difference is below ~10.0 kcal/mol, and the time interval is central at about 16 fs for both AC and CPO. Checking the character of the S_1, T_1, and T_2 states shows that the S_1/T_2 crossing occurs between the $^1n\pi^*$ and $^3\pi\pi^*$ state, which is consistent with El-Sayed's rules.[76] The $S_1/T_2/T_1$ three-state intersection regions have been identified in many carbonyl compounds through various electronic structure calculations.[77–81] Here, we directly see their role in the excited-state nonadiabatic dynamics, and most trajectories undergo ISC to reach the triplet state PESs.

The fourth example (see Figure 9) concerns a direct $S_1 \rightarrow T_1$ path. This type of trajectory is only found rarely (in 5 trajectories). The $S_1 \rightarrow T_1$ hop takes place at 3423.0 fs when there is a large S_1-T_1 SOC of 37.9 cm^{-1} and a small S_1-T_1 energy gap of 4.8 kcal/mol.

Time-dependent state populations. The excited state population is defined as the fraction of trajectories running on the specified excited state PES at a given time. Figure 10 shows the time-dependent populations of the S_0, S_1, T_1 and T_2 state of both AC and CPO**.** The populations show a latency time τ_0 up to which the S_1 state

population remains a constant value of 1. The latency time is the time needed for one trajectory to reach the crossing region and perform the transition to the ground or triplet states. As can be seen in Figure 10(a), the S_1 population exponentially decreases from 1 to 0.10 at ~3000 fs. The S_0 population rises notably faster than the T_1 population before 1200 fs, and after that time the T_1 population increases quickly to 0.6 at about 3000 fs. In CPO (see Figure 10(b)), after the latency time the S_1 population exponentially decreases and reaches 0.10 at 10000 fs. The S_0 population rises notably faster than the T_1 population before 1500 fs, and after that time the T_1 population increases quickly and reaches 0.6 at 9000 fs. Similar to AC, the T_2 population of CPO remains negligible in the whole simulation time.

To obtain the S_1 lifetime, the range from τ_0 to 8000 or 18000 fs of the decay curves in Figure 10 has been fitted, and the fitting details and results were given in the part of S3 and Figure S4 of Supporting Information. For AC, the latency time is 163.5 fs and the delay constant τ_1 is 2156.2 fs, but they become to be 726.5 and 5244.9 fs for CPO. The computed excited state lifetime is composed of both the latency time and the decay constant, thus the S_1 lifetimes are respectively ~2.3 and ~6.0 ps for AC and CPO. The ISC time was also estimated (see Figure S5) to be respectively ~2.3 ps for AC and ~6.4 ps for CPO. Evidently, structural rigid enones, such as CPO in this study, have longer S_1 lifetime and slower ISC rate compared to that of AC and analogous flexible enones, which is consistent with the experimental observations. A lower bound for the S_1 lifetime of AC was determined from linewidth measurements to be 1.8−2.1 ps,[35] and a time constant of 3.5 ps for ISC of the S_1 state of CPO was estimated from the time-resolved photoelectron spectrum.[39]

Distribution of geometrical parameters and SOC at the hopping geometries. Figure 11 shows the distribution of the selected bond-lengths and SOC constants of the geometries at which a hop from S_1 to T_2 or T_1 occurs, and Figure S6 shows the distribution of the O1−C2−C3−C4 dihedral angle. The average geometry of all hops and the optimized MECP geometries were also given in Figures 11 and S6. The bond-lengths are grouped in 0.01 Å increments, and the bond angle in 5° increments.

According to Figures 11(a) and (d), the majority of hopping occurs for the O1−C2 bond-length in the range from 1.29 to 1.45 Å for AC, and from 1.27 to 1.48 Å for CPO. As shown in Figure 11(b) and (e), the majority of hopping occurs for the C3−C4 bond in the range from 1.36 to 1.50 Å for AC, and from 1.35 to 1.55 Å for CPO. As can be seen in Figure S6, both molecules have the same range (150-180°) for the O1−C2−C3−C4 dihedral angle. For AC, though the average hopping C3−C4 bond-length is the same as the MECP geometry, the average hopping O1−C2 bond-length is located at 1.391 Å, about 0.05 Å longer than the MECP geometry. The difference in bond-lengths between the MECP geometry and the average hopping geometry is more pronounced for CPO. These data showed that the geometries that result in hops according to nonadiabatic dynamics are not localized at the MECP, and the true ISC process deviates from the minimum energy path. Additionally, it is noted that these two molecules have nearly the same decay path, since differences in both the O1−C2 and C3−C4 bond-lengths at the average hopping geometries of AC and CPO are small.

Figures 11(c) and (f) show the distribution of SOC of the geometries at which a hop from S_1 to T_2 or T_1 takes place. The SOC are grouped in 1.0 cm^{-1} increments. The average SOC of all hops and the SOC constants at the MECP geometries are also given in Figure 11. According to Figures 11(c) and (f), the majority of hopping occurs for SOC between 36 and 56 cm^{-1} for AC, and between 20 and 45 cm^{-1} for CPO. Also, the distribution of SOC for CPO is more diffuse than that of AC. The SOC constant between S_1 and T_2 at the MECP of AC is 36.7 cm^{-1}, while only 4.4 cm^{-1} at the MECP of CPO. Evidently, the SOC at the MECP geometry of CPO is more largely outside of the range of dynamics simulation than that of AC.

It has been shown that the efficiency of spin inversion is proportional to the SOC matrix element, and inversely proportional to the energy gap.[82] Moreover, efficient spin inversion can be enhanced by motions, which maximize the SOC matrix element and minimize the singlet-triplet separation. According to the calculation results, the S_1, T_1, and T_2 state are generally close in energy from the FC geometry to the S_1

minimum for these two molecules, besides of that both the S_1/T_2 and T_2/T_1 points occur within 5 kcal/mol of the respective $^3n\pi^*$ minimum. In addition, according to the trajectory calculations, the ISC paths of these two molecules are very similar. Thus, the lower ISC rate of CPO can be explained taking into account a smaller SOC constant at the singlet-triplet crossing region. Fast intersystem crossing was observed in the $S_1(n\pi^*)$ state of N-heterocyclic aromatic hydrocarbons and carbonyl compounds, and it is suggested to be primarily mediated by SOC with the $^3\pi\pi^*$ state in the same energy region.[83]

Summary and Conclusion

In the present work, a combination of electronic structure calculations and nonadiabatic dynamics simulations was used to explore the gaseous photodynamics of both AC and CPO. When these two molecules were initially excited into the S_1 state, they relax rapidly toward the more energetically favored geometries via bond alternation of the carbon backbone. After residing on the S_1 surface for some time, the molecules can reach the hot ground state by a S_1/S_0 intersection or undergo ISC to the triplet state PESs. Our dynamics simulations showed that, the $S_1 \rightarrow T_2$ hop occurs in the pecosecond timescale and can efficiently compete with IC to the ground state, which is reasonably consistent with previous experimental results. In addition, we have also observed a few trajectories that decay directly from the S_1 to the T_1 state, but the $S_1 \rightarrow T_1$ is the minor channel for population of the T_1 state compared with the $S_1 \rightarrow T_2$. The important role played by the $S_1/T_2/T_1$ three-state intersection in population of the T_1 state was shown here by direct nonadiabatic dynamics simulations. Since the existence of significant energy barriers to access the relevant conical intersection points to the S_0 state and of energetically close-lying $^3\pi\pi^*$ state over large regions of configuration space, these two molecules undergo efficient ISC with a triplet quantum yield of 0.8, which is consistent with the experimental values.[84,85] The ISC path is also very similar for both molecules. However, CPO has a lower ISC rate owing to the ring constraint that results in a smaller SOC in the singlet-triplet crossing region. The present theoretical study reproduces the

experimental results and gives an explanation about the structural factors that rule the excited-state decay of some types of α,β-enones.

Upon excitation to the S_2 state, however, more decay paths become accessible and they can compete with each other, resulting in a more complex photodynamics. Theoretical calculations on the S_2 state decay of α,β-enones are presently under study.

Acknowledgment

This work was supported by grants from the NSFC (Grant No. 21503047), the Natural Science Foundation of Guizhou Education University (Grant No. 14BS024), and the Provincial Key Disciplines of Guizhou Province (Contract No. ZDXK[2014]18).

Reference:

1 P. Ehrenfreund and S. B. Charnley, *Annu. Rev. Astron. Astrophys.*, 2000, **38**, 427.

2 D. Arntz, A. Fischer, M. Hoeopp, S. Jacobi, J. Sauer, T. Ohara, T. Sato, N. Shimizu and H. Schwind, *Acrolein and Methacrolein*, Wiley-VCH Verlag GmbH & Co. KGaA: Weinheim, Germany, 2012.

3 J. Pan, B. Awoyemi, Z. Xuan, P. Vohra, H.-T. Wang, M. Dyba, E. Greenspan, Y. Fu, K. Creswell, L. Zhang, D. Berry, M.-S. Tang and F.-L. Chung, *Chem. Res. Toxicol.*, 2012, **25**, 2788.

4 D. Chen, L. Fang, H. Li, M. Tang and C. Jin, *J. Biol. Chem.*, 2013, **288**, 21678.

5 D. I. Schuster, *The chemistry of enones*, edited by S. Patai and Z. Rappoport Ch. 15, Wiley, Chichester UK, 1989.

6 D. I. Schuster, *CRC Handbook Of Organic Photochemistry And Photobiology, Volumes 1 & 2, Second Edition*, edited by W. Horspool and F. Lenci Ch. 72, CRC Press, 2003.

7 J. W. Coomber and J. N. Pitts, Jr., *J. Am. Chem. Soc.*, 1969, **91**, 547.

8 E. P. Gardner, P. D. Sperry and J. G. Calvert, *J. Phys. Chem.*, 1987, **91**, 1922.

9 S.-H. Jen and I.-C. Chen, *J. Chem. Phys.*, 1999, **111**, 8448.

10 M. E. Umstead, R. G. Shortridge and M. C. Lin, *J. Phys. Chem.*, 1978, **82**, 1455.

11 H. Shinohara and N. Nishi, *J. Chem. Phys.*, 1982, **77**, 234.

12 G. T. Fujimoto, M. E. Umstead and M. C. Lin, *J. Chem. Phys.*, 1985, **82**, 3042.

13 B. M. Haas, T. K. Minton, P. Felder and J. R. Huber, *J. Phys. Chem.*, 1991, **95**, 5149.

14 P. C. Lessard and R. N. Rosenfeld, *J. Phys. Chem.*, 1992, **96**, 4615.

15 Y. T. Kao, W. C. Chen, C. H. Yu and I. C. Chen, *J. Chem. Phys.*, 2001, **114**, 8964.

16 B. F. Parsons, D. E. Szpumar and L. J. Butler, *J. Chem. Phys.*, 2002, **117**, 7889.

17 O. Geβner, E. t.-H. Chrysostom, A. M. D. Lee, D. M. Wardlaw, M.-L. Ho, S.-J. Lee, B.-M. Cheng, M. Z. Zgierski, I.-C. Chen, J. P. Shaffer, C. C. Hayden and A. Stolow, *Faraday Discuss.*, 2004, **127**, 193.

18 S.-H. Lee, J. J. Lin, and Y. T. Lee, *J. Electron Spectrosc. Relat. Phenom.*, 2005, **144**, 135.

19 C. Chaudhuri and S.-H. Lee, *Phys. Chem. Chem. Phys.*, 2011, **13**, 7312.

20 W.-H. Fang, *J. Am. Chem. Soc.*, 1999, **121**, 8376.

21 M. Reguero, M. Olivucci, F. Bernardi and M. A. Robb, *J. Am. Chem. Soc.*, 1994, **116**, 2103.

22 W. Wu, C. Yang, H. Zhao, K. Liu and H. Su, *J. Chem. Phys.*, 2010, **132**, 124510.

23 P. Eaton, *Acc. Chem. Res.*, 1968, **1**, 50, and references cited therein.

24 M. T. Crimmins, *Chem. Rev.*, 1988, **88**, 1453.

25 D. I. Schuster, G. Lem and N. A. Kapriidis, *Chem. Rev.*, 1993, **9**3, 3.

26 D. Andrew, A. C. Weedon, *J. Am. Chem. Soc.*, 1995, **117**, 5647.

27 L. A. Paquette, Z. Zhao, F. Gallou and J. Liu, *J. Am. Chem. Soc.*, 2000, **122**, 1540.

28 A. D. Cohen, B. M. Showalter, D. A. Brady, C. A. Kenesky and J. P. Toscano, *Phys. Chem. Chem. Phys.*, 2003, **5**, 1059.

29 R. Bonneau, *J. Am. Chem. Soc.*, 1980, **102**, 3816.

30 A. Devaquet, *J. Am. Chem. Soc.*, 1972, **94**, 5160.

31 M.-D. Su, *Chem. Phys.*, 1996, **205**, 277.

32 E. Garcia-Exposito, M. J. Bearpark, R. M. Ortuno, V. Branchdell, M. A. Robb and S. Wilsey, J. Org. Chem. *J. Org. Chem.*, 2001, **66**, 8811.

33 E. García-Expósito, M. J. Bearpark, R. M. Ortuno, M. A. Robb and V. Branchadell, *J. Org. Chem.*, 2002, **67**, 6070.

34 R. S. Becker, K. Inuzuka and J. King, *J. Chem. Phys.*, 1970, **52**, 5164.

35 K. W. Paulisse, T. O. Friday, M. L. Graske and M. F. Polik, *J. Chem. Phys.*, 2000, **113**, 184.

36 A. M. D. Lee, J. D. Coe, S. Ullrich, M.-L. Ho, S.-J. Lee, B.-M. Cheng, M. Z. Zgierski, I.-C. Chen, T. J. Martinez and A. Stolow, *J. Phys. Chem. A*, 2007, **111**, 11948.

37 O. Schalk, P. Lang, M. S. Schuurman, G. Wu, M. Bradler, E. Riedle and A. Stolow, *EPJ Web of Conferences*, 2013, **41**, 05029.

38 E. Riedle, M. Bradler, C. Sailer, M. Wenninger and I. Pugliesi, *Faraday Discuss.*, 2013, **163**, 139.

39 O. Schalk, M. S. Schuurman, G. Wu, P. Lang, M. Mucke, R. Feifel and A. Stolow, *J. Phys. Chem. A*, 2014, **118**, 2279.

40 I. N. Ragazos, M. A. Robb, F. Bernardi and M. Olivucci, *Chem. Phys. Lett.*, 1992, **197**, 217.

41 M. J. Bearpark, M. A. Robb and H. B. Schlegel, *Chem. Phys. Lett.*, 1994, **223**, 269.

42 M. J. Frisch, G. W. Trucks, H. B. Schlegel et al., *GAUSSIAN 09, Revision A.2*, Gaussian, Inc., Wallingford CT, 2009.

43 H.-J. Werner, P. J. Knowles, F. R. Manby, M. Schutz et al., *MOLPRO, version 2010.1, a package of ab initio programs, 2010*, see http://www.molpro.net.

44 C. Marian and U. Wahlgren, *Chem. Phys. Lett.*, 1996, **251**, 357.

45 B. Hess, C. Marian, U. Wahlgren and O. Gropen, *Chem. Phys. Lett.*, 1996, **251**, 365.

46 B. O. Roos, *Ab Initio Methods in Quantum Chemistry, Part 2*, edited by K. P. Lawley pp.399-446, Wiley, Chichester UK, 1987.

47 K. Andersson, P.-A. Malmqvist, B. O. Roos, A. J. Sadlej and K.Wolinski, *J. Phys. Chem.*, 1990, **94**, 5483.

48 K. Andersson, P.-A. Malmqvist and B. O. Roos, *J. Chem. Phys.*, 1992, **96**, 1218.

49 Molcas 7.4: F. Aquilante, L. De Vico, N. Ferre, G. Ghigo, P.-A Malmqvist, P. Neogrady, T.B. Pedersen, M. Pitonak, M. Reiher, B. O. Roos, L. Serrano-Andres, M.

Urban, V. Veryazov and R. Lindh, *J. Comput. Chem.*, 2010, **31**, 224. Code development: V. Veryazov, P.-O. Widmark, L. Serrano-Andres, R. Lindh and B. O. Roos, *Int. J. Quantum Chem.*, 2004, **100**, 626. Molcas 7: G. Karlstrom, R. Lindh, P.-A. Malmqvist, B. O. Roos, U. Ryde, V. Veryazov, P.-O. Widmark, M. Cossi, B. Schimmelpfennig, P. Neograd y and L. Seijo, *Comp. Mater. Sci.*, 2003, **28**, 222.

50 J. Finley, P.-A. Malmqvist, B. O. Roos and L. Serrano-Andres, *Chem. Phys. Lett.*, 1998, **288**, 299.

51 N. Fosberg and P. Malmqvist, *Chem. Phys. Lett.*, 1997, **274**, 196.

52 J. Cao, Q. Fang and W.-H. Fang, *J. Chem. Phys.*, 2011, **134**, 044307.

53 J. Cao, L.-H. Liu, W.-H. Fang, Z.-Z. Xie and Y. Zhang, *J. Chem. Phys.*, 2013, **138**, 134306.

54 J. C. Tully, *J. Chem. Phys.*, 1990, **93**, 1061.

55 Y. Amatatsu, K. Morokuma and S. Yabushita, *J. Chem. Phys.*, 1991, **94**, 4858.

56 A. Marks and D. Thompson, *J. Chem. Phys.*, 1991, **95**, 8056.

57 T. Takayanagi, *J. Phys. Chem. A*, 2002, **106**, 4914.

58 B. Maiti, G. Schatz and G. Lendvay, *J. Phys. Chem. A*, 2004, **108**, 8772.

59 R. Valero and D. Truhlar, *J. Phys. Chem. A*, 2007, **111**, 8536.

60 W. Hu, G. Lendvay, B. Maiti and G. Schatz, *J. Phys. Chem. A*, 2008, **112**, 2093.

61 R. Valero, D. Truhlar and A. Jasper, *J. Phys. Chem. A*, 2008, **112**, 5756.

62 B. Li and K. Han, *J. Phys. Chem. A*, 2009, **113**, 10189.

63 K. Rajak and B. Maiti, *J. Chem. Phys.*, 2010, **133**, 011101.

64 B. Han and Y. Zheng, *J. Comput. Chem.*, 2011, **32**, 3520.

65 B. Fu, B. Shepler and J. Bowman, *J. Am. Chem. Soc.*, 2011, **133**, 7957.

66 G. Granucci, M. Persico and G. Spighi, *J. Chem. Phys.*, 2012, **137**, 22A501.

67 L. Favero, G. Granucci and M. Persico, *Phys. Chem. Chem. Phys.*, 2013, **15**, 20651.

68 L. Martínez-Fernández, I. Corral, G. Granucci and M. Persico, *Chem. Sci.*, 2014, **5**, 1336.

69 G.-L. Cui and Walter Thiel, *J. Chem. Phys.*, 2014, **141**, 124101.

70 M. Richter, P. Marquetand, J. Gonzalez-Vazquez, I. Sola and L. Gonzalez, *J. Chem. Theory Comput.*, 2011, **7**, 1253.

71 M. Richter, P. Marquetand, J. González-Vázquez, I. Sola and L. González, *J. Phys. Chem. Lett.*, 2012, **3**, 3090.

72 S. Mai, P. Marquetand and L. González, *J. Chem. Phys.*, 2014, **140**, 204302.

73 C. E. Blom, G. Grassi and A. Bauder, *J. Am. Chem. Soc.*, 1984, **106**, 7427.

74 R. Ruoff, A. Krebs, T. Schaeffer, G. Stiegler and H.-K. Bodenseh, *J. Mol. Struct.* 1997, **407**, 93.

75 H. E. Zimmerman, *Tetrahedron*, 1974, **30**, 1617.

76 M. A. El-Sayed, *J. Chem. Phys.*, 1963, **38**, 2834.

77 W.-H. Fang and D. Phillips, *ChemPhysChem*, 2002, **3**, 889.

78 W.-H. Fang, *Acc. Chem. Res.*, 2008, **41**, 452.

79 G.-L. Cui, Y. Lu and W. Thiel, *Chem. Phys. Lett.*, 2012, **537**, 21.

80 M. Huix-Rotllant, D. Siri and N. Ferré, *Phys. Chem. Chem. Phys.*, 2013, **15**, 19293.

81 Q. Ou and J. Subotnik, *J. Phys. Chem. C*, 2013, **117**, 19839.

82 S. P. McGlynn, T. Azumi and M. Kinoshita, *The triplet state*, Prentice-Hall, New York, 1969.

83 M. Baba, *J. Phys. Chem. A*, 2011, **115**, 9514.

84 J. L. Ruhlen and P. A. Leermakers, *J. Am. Chem. Soc.*, 1967, **89**, 4944.

85 R. Bonneau, *J. Am. Chem. Soc.*, 1980, **102**, 3816.

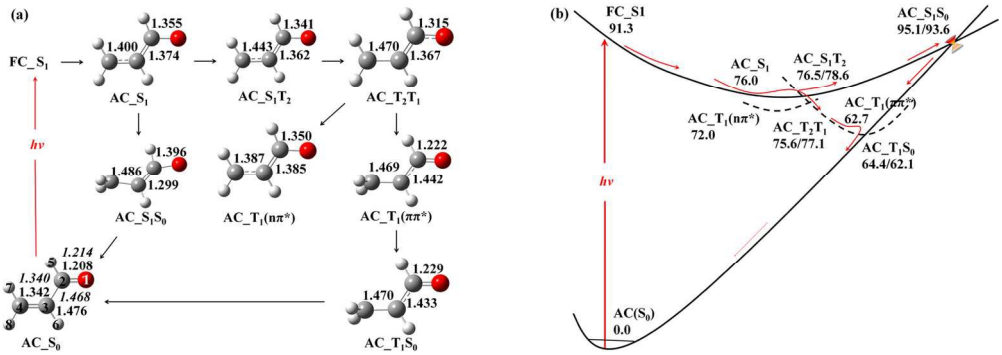

171x60mm (300 x 300 DPI)

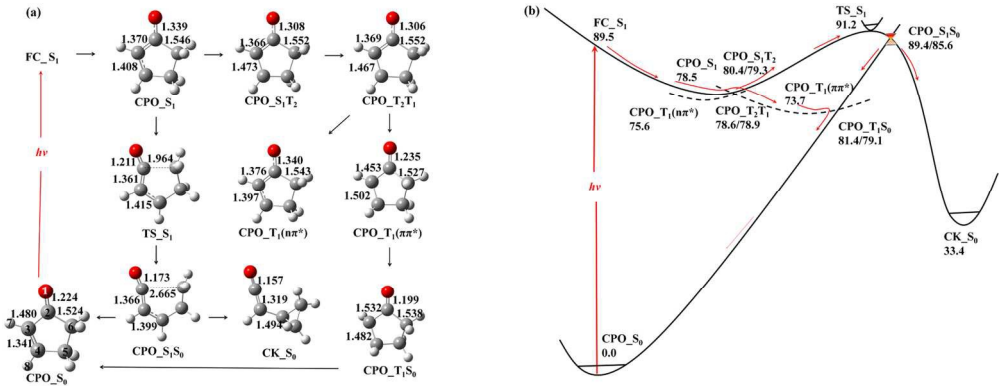

171x66mm (300 x 300 DPI)

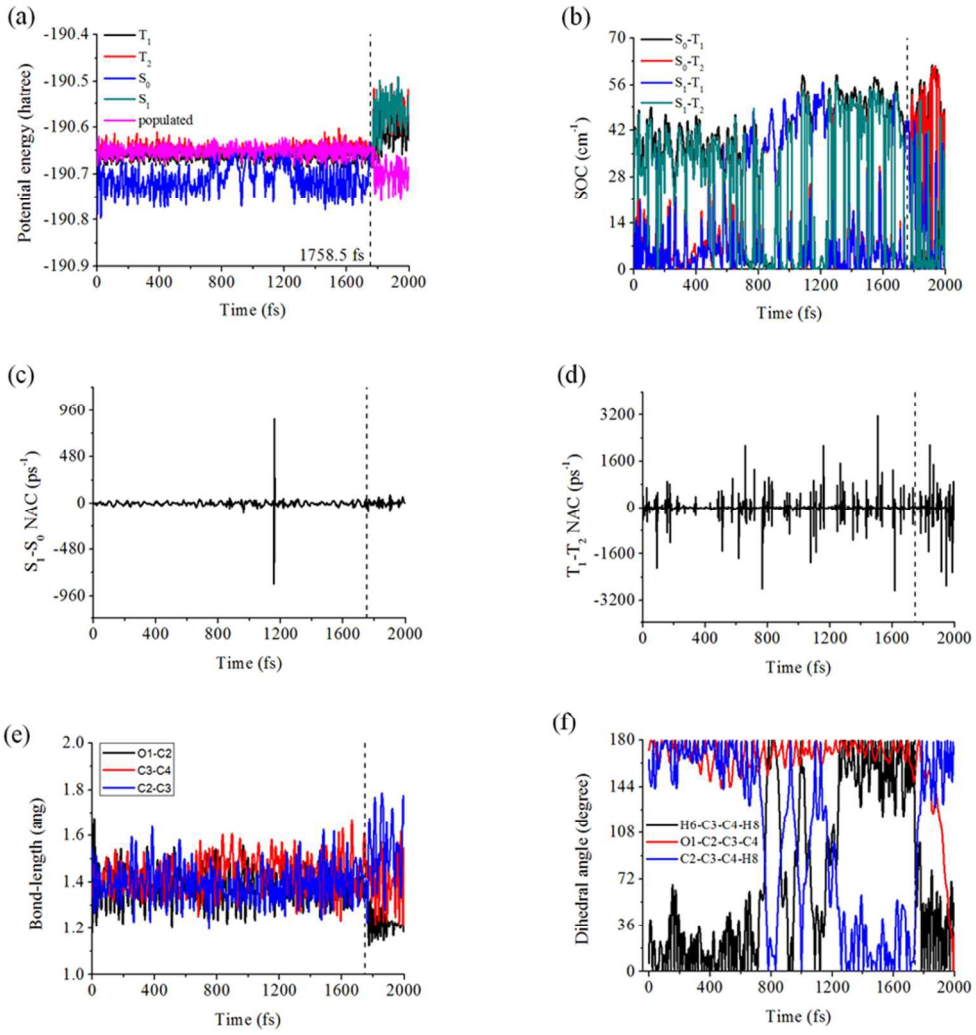

82x86mm (300 x 300 DPI)

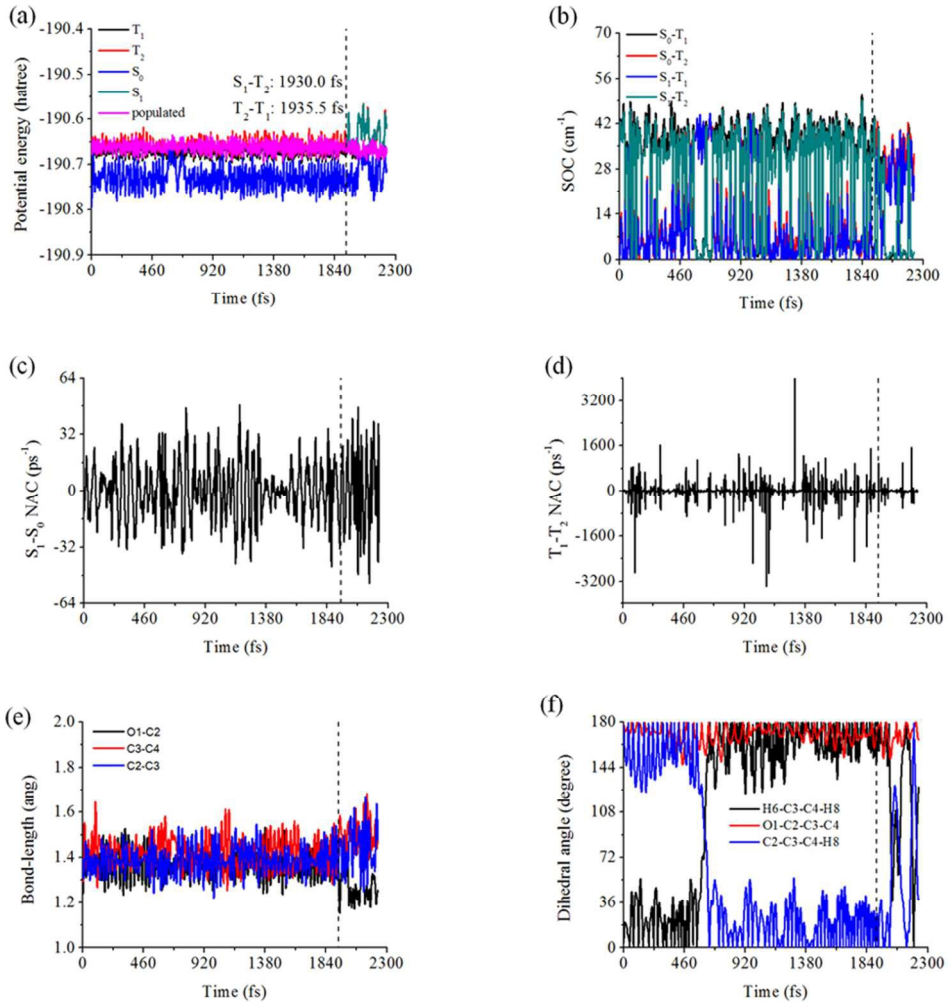

82x83mm (300 x 300 DPI)

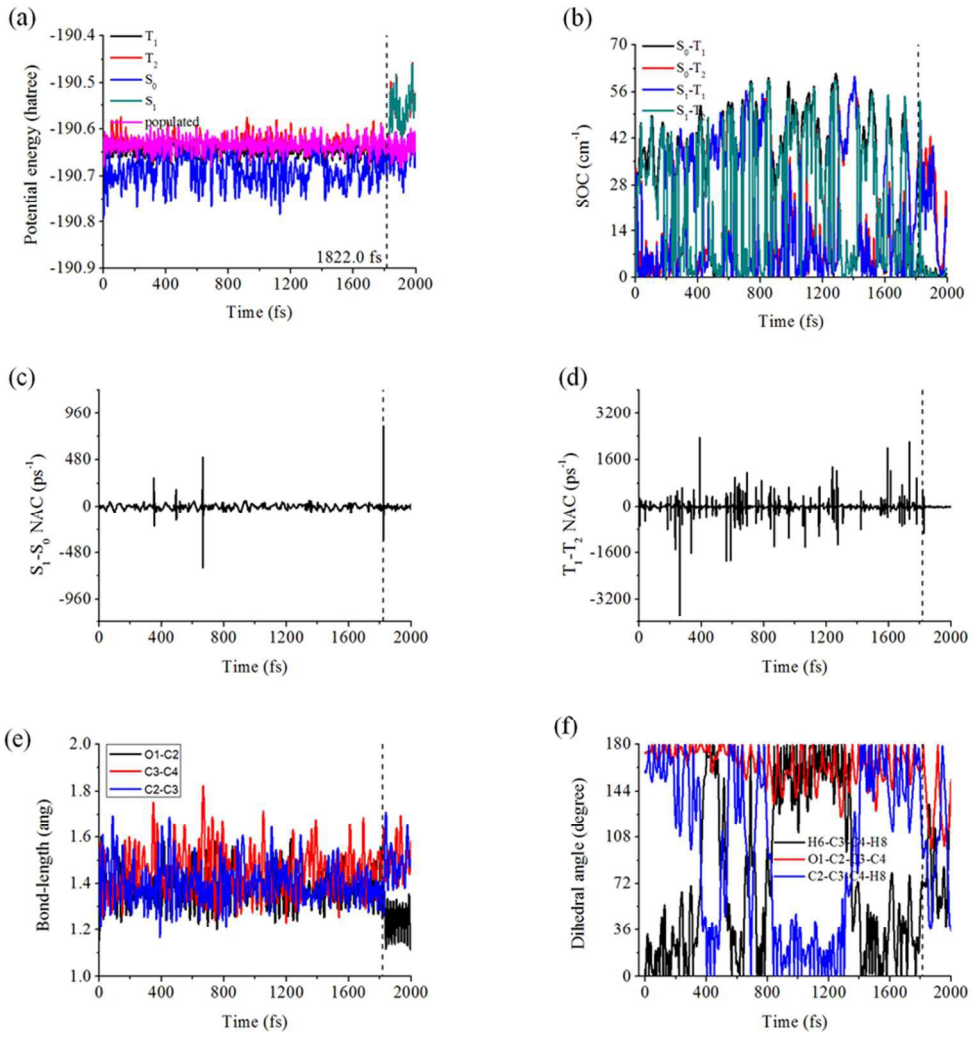

82x85mm (300 x 300 DPI)

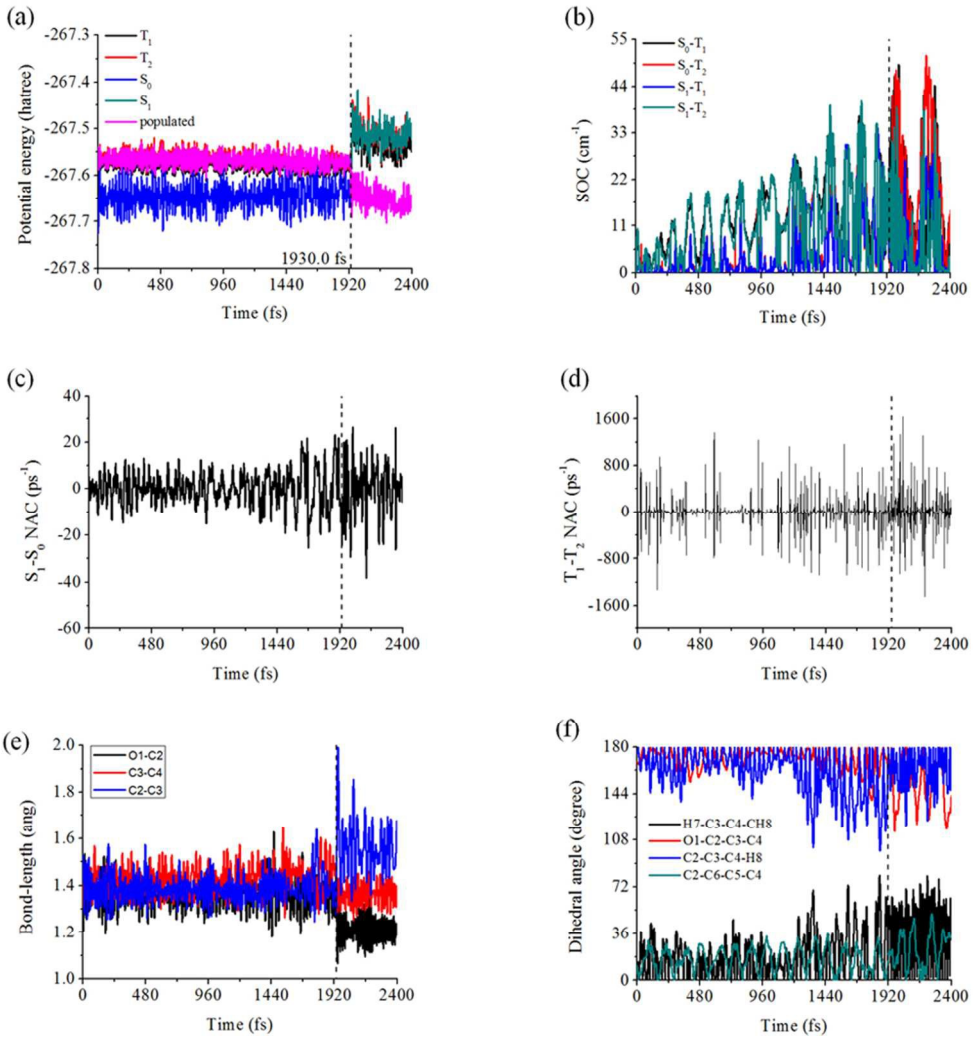

82x86mm (300 x 300 DPI)

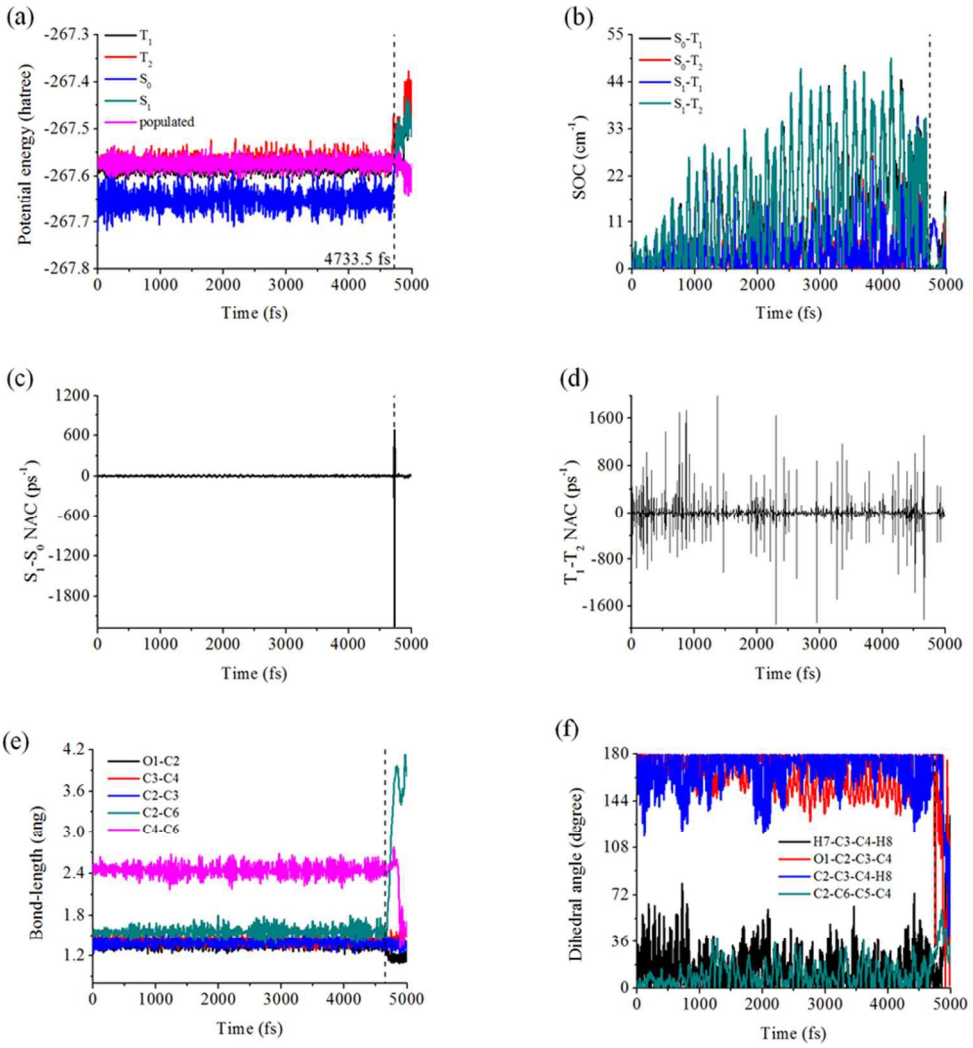

82x87mm (300 x 300 DPI)

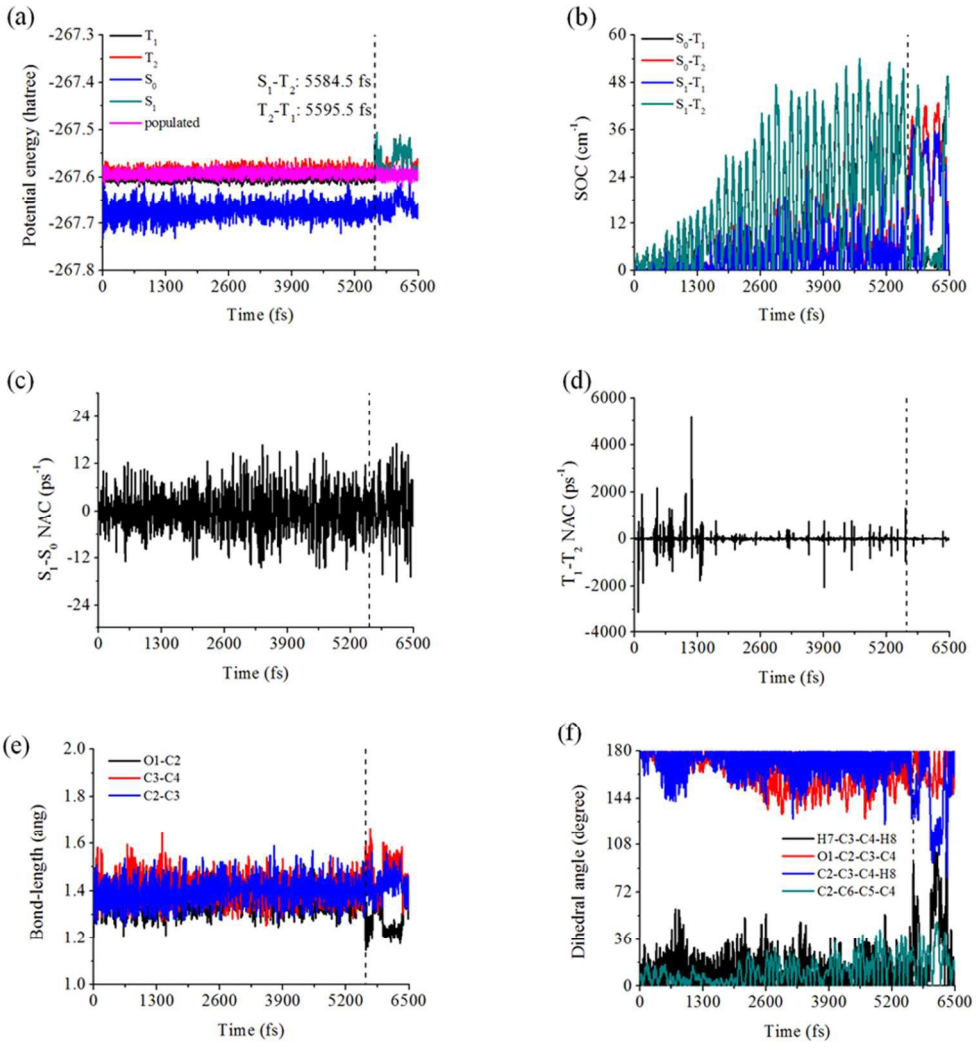

82x87mm (300 x 300 DPI)

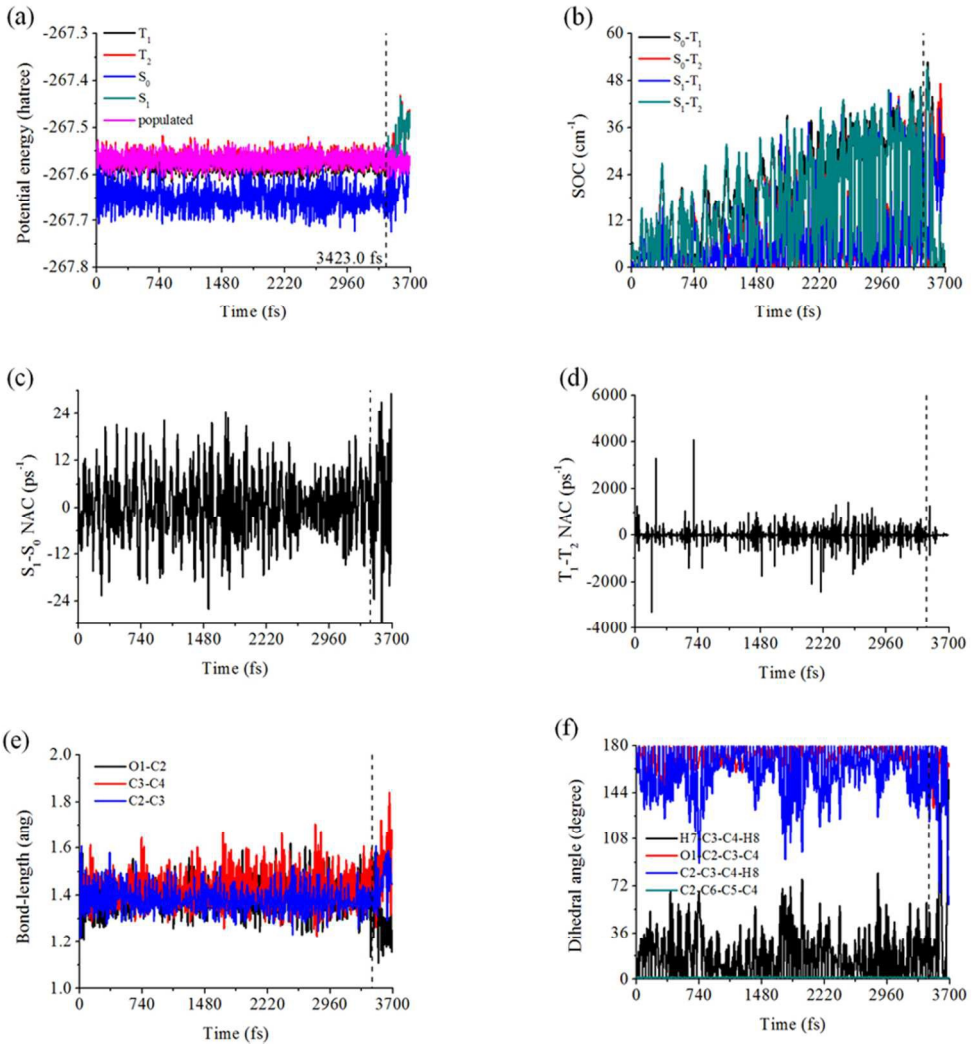

82x87mm (300 x 300 DPI)

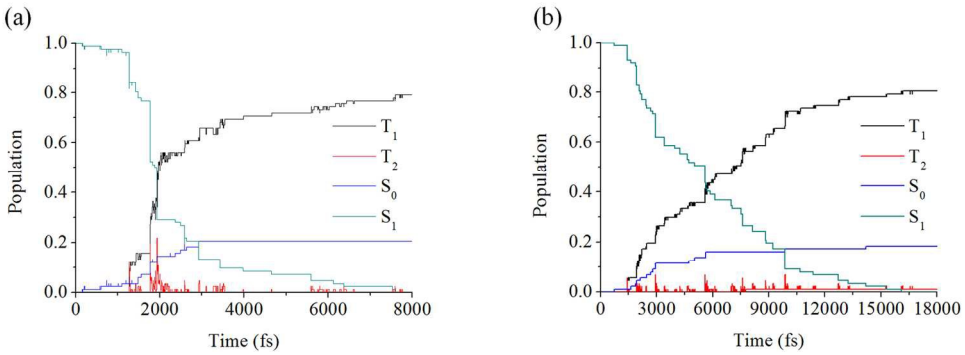

171x61mm (300 x 300 DPI)

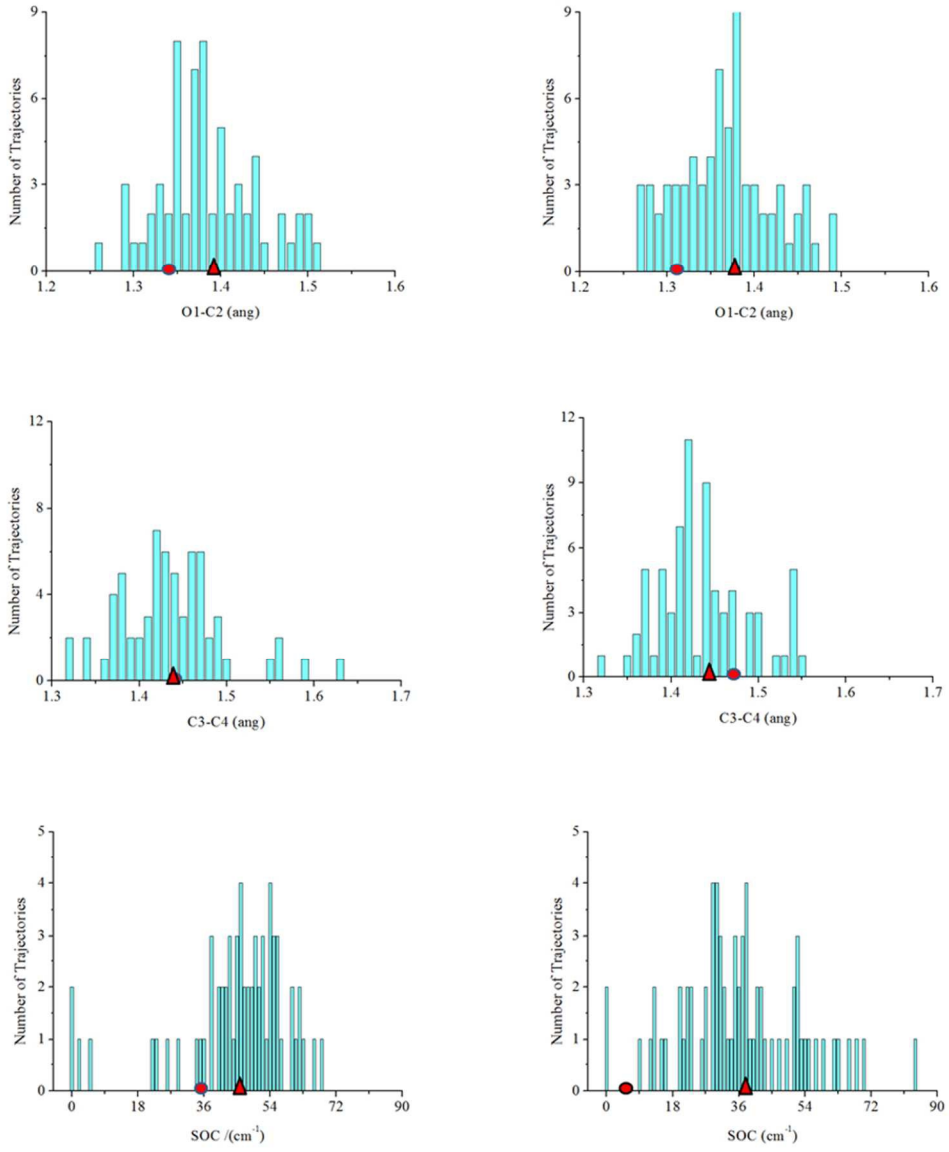

82x98mm (300 x 300 DPI)